Journal of Power Sources 244 (2013) 312–317

Contents lists available at SciVerse ScienceDirect

Journal of Power Sources

journal homepage: www.elsevier.com/locate/jpowsour

Improvement of solid-state symmetric cell performance with lithium vanadium phosphate

Eiji Kobayashi [a], Ayuko Kitajou [b], Shigeto Okada [a,*], Jun-ichi Yamaki [a]

[a] Interdisciplinary Graduate School of Engineering Sciences, Kyushu University, 6-1 Kasuga-koen, Kasuga 816-8580, Japan
[b] Research and Education Center of Carbon Resources, Kyushu University, 6-1 Kasuga-koen, Kasuga 816-8580, Japan

HIGHLIGHTS

- $Li_3V_2(PO_4)_3/Li_{1.5}Al_{0.5}Ge_{1.5}(PO_4)_3/Li_3V_2(PO_4)_3$ all solid-state Li-ion battery was made.
- The key concept to reduce the contact resistivity is common NASICON structure.
- The capacity per cathode weight for the all-solid-state battery achieved 92 mAh g^{-1} even at RT.

ARTICLE INFO

Article history:
Received 28 October 2012
Received in revised form
18 December 2012
Accepted 4 January 2013
Available online 12 January 2013

Keywords:
Li-ion batteries
Solid electrolyte
Symmetric battery
All-solid-state battery

ABSTRACT

We constructed a $Li_3V_2(PO_4)_3/Li_{1.5}Al_{0.5}Ge_{1.5}(PO_4)_3/Li_3V_2(PO_4)_3$ symmetric all solid-state Li-ion battery. Since the rechargeable capacity of $Li_{3+x}V_2(PO_4)_3$ anode is lower than that of $Li_{3-x}V_2(PO_4)_3$ cathode, the symmetric cell capacity is restricted by the anode capacity. So, the improvement of $Li_{3+x}V_2(PO_4)_3$ anode properties was tried using mechanical milling to uniformly mix $Li_3V_2(PO_4)_3$ and carbon. The charge and discharge capacity of $Li_3V_2(PO_4)_3$/C using mechanical milling was greatly increased compared to $Li_3V_2(PO_4)_3$/C using hand milling. The structure change with the insertion and extraction of lithium confirmed using *ex-situ* XRD measurements. The Li extraction/insertion of $Li_3V_2(PO_4)_3$ with a NASICON structure can proceed to the reversible expansion/contraction of the lattice due to the structural strength and flexibility of NASICON framework with the corner-sharing matrix. The discharge capacity of the all solid-state battery per $Li_3V_2(PO_4)_3$ in cathode weight achieved 92 mAh g^{-1} by good dispersion state of $Li_3V_2(PO_4)_3$ and carbon using mechanical milling.

1. Introduction

Lithium-ion batteries have been used as compact power sources in portable devices. However, before Li-ion batteries can be used as large-scale power sources in electric vehicles, their performance needs to be improved with regard to battery cycle life, production costs and safety. In particular, several safety issues must be addressed to make Li-ion batteries suitable as reliable power sources. One Li-ion battery safety issue is that at elevated temperatures, charged oxide cathodes such as Li_xCoO_2 easily release oxygen gas, which could react with organic electrolytes exothermally [1,2]. To improve the safety of Li-ion batteries, the thermal stabilities of the electrodes and electrolyte needs to be enhanced by suppressing these exothermic reactions. All solid-state Li-ion batteries, which use an incombustible solid electrolyte instead of an organic liquid electrolyte, have been proposed as strong candidates for such safety-sensitive batteries.

A number of studies have reported on all solid-state Li-ion batteries using glass ceramics, which have high Li-ion conductivity, such as $Li_{1+x+y}Al_xTi_{2-x}Si_yP_{3-y}O_{12}$, $80Li_2S{-}20P_2O_5$, and $Li_{10}GeP_2S_{12}$ [3–5]. As reported, all solid-state Li-ion batteries, $Li_{4/3}Ti_{5/3}O_4/Li_{1+x+y}Al_xTi_{2-x}Si_yP_{3-y}O_{12}/LiCoO_2$ cell gave a discharge capacity of 150 mAh g^{-1} at 1/12 C rate at 60 °C [6]. $In/80Li_2O{-}20P_2S_5/LiCoO_2$ cell showed a reversible capacity of 75 mAh g^{-1} at 1.3 mA cm^{-2} at room temperature [7]. However, the ionic conductivity of a solid electrolyte is lower than that of a liquid electrolyte, and the former shows a larger interfacial resistance with the other solid components such as the electrode. Hence, solid electrolytes cannot be easily put into practical use.

We developed all solid-state Li-ion batteries that use NASICON-type materials for both the electrolyte and the electrodes;

* Corresponding author. Institute for Materials Chemistry and Engineering, Kyushu University, 6-1 Kasuga-koen, Kasuga 816-8580, Japan. Tel./fax: +81 92 583 7841.
E-mail addresses: s-okada@cm.kyushu-u.ac.jp, s-okada@mx3.canvas.ne.jp (S. Okada).

0378-7753/$ – see front matter © 2013 Elsevier B.V. All rights reserved.
http://dx.doi.org/10.1016/j.jpowsour.2013.01.031

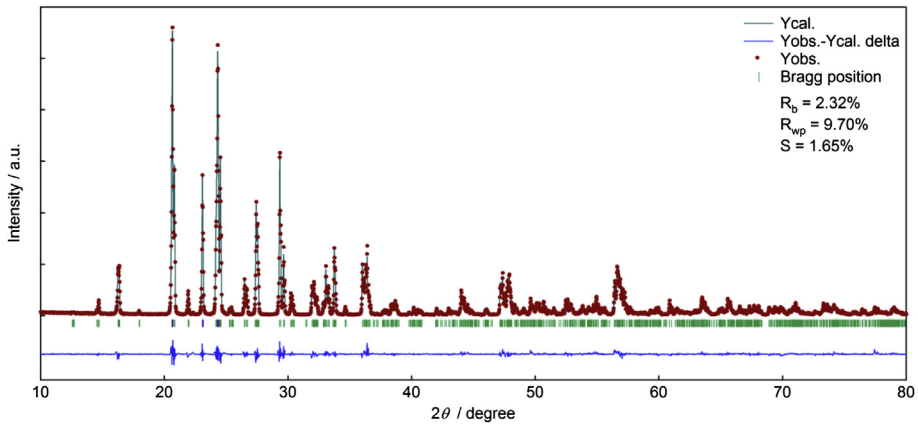

Fig. 1. Observed (dot) and calculated (solid line) X-ray diffraction profile of $Li_3V_2(PO_4)_3$ (LVP). The difference between observed and calculated profiles is plotted below.

specifically, $Li_{1.5}Al_{0.5}Ge_{1.5}(PO_4)_3$ (LAGP) and $Li_3V_2(PO_4)_3$ (LVP) were used for the solid electrolyte and the electrodes, respectively [8]. NASICON-type LAGP has been known as a fast Li-ion conductor, and Li-ion conductivity is 2.4×10^{-4} S cm^{-1} at room temperature [9]. In addition, NASICON-type LVP is also promising cathode material for Li-ion batteries [10]. The reaction formulas for Li insertion/extraction of LVP are as follows [11];

$Li_3V_2(PO_4)_3 \rightarrow LiV_2(PO_4)_3 + 2Li^+ + 2e^-$ (around 4.1 V, V^{+3}/V^{+4} redox couple)

$Li_3V_2(PO_4)_3 + 2Li^+ + 2e^- \rightarrow Li_5V_2(PO_4)_3$ (around 1.7 V, V^{+2}/V^{+3} redox couple)

Therefore, LVP can be used as both cathode and anode active materials for the symmetrical cell. Such a symmetrical cell has some unique advantages: (1) it can be discharged down to 0 V, (2) the cell volume change can be compensated by the opposite behavior of the cathode and anode electrode, and (3) the processing costs of the coating electrode can be reduced by dip coating. However, the first discharge capacities of LVP/LAGP/LVP all solid-state Li-ion batteries at 25 °C is 42 mAh g^{-1}, which corresponds to 32% of the theory based on the assumption that $2Li^+$ reacts with LVP (132 mAh g^{-1}), at a rate of 0.2 mA cm^{-2}. This suggested that the Li-ion battery has large internal resistance, and the redox couple of V^{+2}/V^{+3} for LVP has a large irreversible capacity due to quite low electroconductivity.

In this paper, the improvement of electroconductivity for $Li_3V_2(PO_4)_3$ anode properties was tried using mechanical milling to mix $Li_3V_2(PO_4)_3$ and carbon, uniformly. In addition, we investigated the anode properties and structure changes during the first charge–discharge cycle. The electrochemical properties of the LVP/LAGP/LVP all solid-state Li-ion batteries were improved based on the obtained results.

2. Experimental

LVP and LAGP were synthesized according to the previous reports [8,10]. LVP was prepared from a mixture of very pure Li_2CO_3 (Wako Pure Chemical Industries), V_2O_5 (Nacalai Tesque) and $NH_4H_2PO_4$ (Wako) powders with the cationic ratio of Li:V:PO_4 = 3:2:3. The mixture was sintered at 300 °C for 2 h under Ar atmosphere. The sintered mixture was ground, and was again sintered at 860 °C for 12 h under a mix gas (Ar + 5% H_2).

The crystalline LAGP was prepared from a mixture of Li_2CO_3, GeO_2 (Shinko Chemical), $NH_4H_2PO_4$, and Al_2O_3 (Nippon Light Metal) at a stoichiometric ratio. The mixture was sintered at 500 °C for 2 h in air using an electric oven. The sintered mixture was ground, and was sintered again at 800 °C followed by sintering at 900 °C for 2 h in air. To prepare amorphous LAGP, the crystalline powder was place in a Pt crucible and heated in a furnace at 1200 °C for 1 h in air. The melted LAGP was quenched in ice water, still in a Pt crucible. The obtained materials were identified by X-ray diffraction (XRD, RINT2100HLR/PC, Rigaku; Cu-Kα, 50 kV, 300 mA).

The 70 wt.% obtained LVP powder was hand milled and dry ball milled with 25 wt.% acetylene black (AB, Denki Kagaku Co.) in air. Cathodes were prepared by mixing the LVP/C composite powder with a 5 wt.% PTFE binder (Polyflon PTFE F-103, Daikin Industries). The electrochemical performance of the LVP was evaluated with a 2032 coin-type cell using a non-aqueous electrolyte (1 M $LiPF_6$/EC + DMC (1:1 in volume), Kishida Chemical Co.) and a polypropylene separator (Celgard 3501) against Li metal (Honjo Metal Co.).

All of the cells were assembled in an Ar-filled glove box. The charge–discharge measurement was performed in galvanostatic mode at a rate of 7.5 mA g^{-1} (0.2 mA cm^{-2}) in the potential window between 1.5 and 3.0 V. The test temperature was 25 °C. The electrodes were carefully taken out from the cells in the Ar-filled glove box, washed, and immersed in dimethyl carbonate (DMC) for one night to remove the electrolyte, and dried prior to being set in an Ar-filled cell for XRD.

The solid electrolyte was prepared by pressing crystalline LAGP powder at 49 MPa into a pellet with a diameter of 16 mm and thickness of 0.5 mm. The pellet was heated at 840 °C for 2 h in air. The electrode was made from LVP (49 wt.%), amorphous LAGP (49 wt.%) and vapor-grown carbon fiber (VGCF, Showa Denko; 2 wt.%). To increase the interface area between the active materials of LVP and the LAGP electrolyte, we used not crystallized but

Table 1
The structural parameters and selected interatomic distance in LVP compounds.

Structural formula	$Li_3V_2(PO_4)_3$		R_b = 2.32%
Crystal system	Monoclinic		R_{wp} = 9.70%
Space group	$P2_1/n$		S = 1.65%
Lattice parameters			
a (Å)	b (Å)	c (Å)	β (°)	V (Å^3)
8.6620(6)	8.6470(2)	12.1150(0)	90.593(8)	907.376(9)
V–O bond length (Å)			
V1–O1	2.00(8)	V2–O2	2.01(9)
V1–O3	2.06(8)	V2–O4	2.17(5)
V1–O6	1.86(2)	V2–O5	1.89(5)
V1–O7	1.98(8)	V2–O8	1.98(3)
V1–O9	1.98(7)	V2–O10	1.87(2)
V1–O11	2.03(9)	V2–O12	2.06(7)

amorphous LAGP, which was added to the LVP powder. The mixture (97 wt.%) was added to BL-S polyvinyl alkyl acetyl alcohol (BL-S, Sekisui Chemical Co.; 3 wt.%) and 2,2,4-trimethyl-2,4-pentanediol mono isobutyrate (CS-12, Chisso Corp.).

The slurry was screen-printed on both sides of the LAGP pellets, and then was heated at 600 °C for 40 h by hot pressing in Ar atmosphere. Fractured cross-sections of the resultant pellets were observed by scanning electron microscopy (SEM) to evaluate the thickness of the electrode. The surface of the pellet was analyzed by XRD. The pellets were sealed in a coin-type cell after drying at 110 °C overnight in a vacuum. The charge–discharge measurement was performed in galvanostatic mode at a rate of 6.1 mA g^{-1} (8.8 μA cm^{-2}) in the potential window between 0 and 2.4 V at 25 °C.

3. Results and discussion

3.1. Characterization of obtained LVP

The XRD pattern of LVP confirms that the sample is pure phase and well crystallized. Fig. 1 shows the Rietveld refinement result, and the crystal parameters are summarized in Table 1 [12]. All diffraction peaks are indexed in a monoclinic system with the space group $P2_1/n$. The cell parameters $a = 8.6620(6)$ Å, $b = 8.6470(2)$ Å, $c = 12.1150(0)$ Å and $\beta = 90.593(8)$ obtained from the refinement are in good agreement with previously reported values [13]. The structure consists of a 3D framework of VO_6 octahedra and PO_4 tetrahedra sharing common corner oxygens. Based on the bond distance calculation, it is found that the vanadium atoms are located in the distorted VO_6 octahedra, with the V–O distances ranging from 1.86 to 2.17 Å.

3.2. Electrochemical properties of LVP against Li anode with non-aqueous electrolyte

Fig. 2a shows the cathode properties (V^{3+}/V^{4+} redox couple) of the carbon-coated LVP using mechanical milling (LVP/C-MM) and hand milling (LVP/C-HM) in the potential window between 3.0 and 4.2 V. The LVP/C-MM showed the initial charge (Li^+ extracted) and discharge (Li^+ inserted) capacities of 137 mAh g^{-1} and 122 mAh g^{-1}, respectively, with an 89% discharge/charge efficiency, whereas the initial charge and discharge capacities of LVP/C-HM were 116 mAh g^{-1} and 97 mAh g^{-1}, respectively, with an 84% discharge/charge efficiency.

On the other hand, Fig. 2b shows the anode properties (V^{2+}/V^{3+} redox couple) of LVP/C-HM and LVP/C-MM in the potential window between 1.5 and 3.0 V. The first discharge (Li^+ inserted) and charge (Li^+ extracted) of LVP/C-HM were 64 mAh g^{-1} and 28 mAh g^{-1}, respectively, and LVP/C-HM had the large irreversible capacity at 36 mAh g^{-1}. In contrast, the first discharge and charge of LVP/C-MM were 135 mAh g^{-1} and 109 mAh g^{-1}, respectively. The theoretical capacity was achieved experimentally, with the complete reduction of the V^{3+} ions into V^{2+} ions. During the first discharge process at LVP/C-MM, the cell voltage gradually decreased down to 1.5 V through an inflection point around 1.9 and 1.7 V at a rate of 7.5 mA g^{-1} (0.2 mA cm^{-2}). These discharge reaction formulas for Li insertion into LVP are as follows [11];

$$Li_3V_2(PO_4)_3 + 0.5Li^+ + 0.5e^- \geq Li_{3.5}V_2(PO_4)_3 \ (1.95\ V)$$

$$Li_{3.5}V_2(PO_4)_3 + 0.5Li^+ + 0.5e^- \geq Li_4V_2(PO_4)_3 \ (1.86\ V)$$

$$Li_4V_2(PO_4)_3 + 0.5Li^+ + 0.5e^- \geq Li_{4.5}V_2(PO_4)_3 \ (1.74\ V)$$

$$Li_{4.5}V_2(PO_4)_3 + 0.5Li^+ + 0.5e^- \geq Li_5V_2(PO_4)_3 \ (1.66\ V)$$

In addition, the charge and discharge voltage of LVP/C-MM were higher than those of LVP/C-HM, and the overpotential of LVP/C-MM was also smaller than that of LVP/C-HM. These results suggested that the electroconductivity of LVP has been improved by increasing the connected area due to uniformly mixed LVP and carbon.

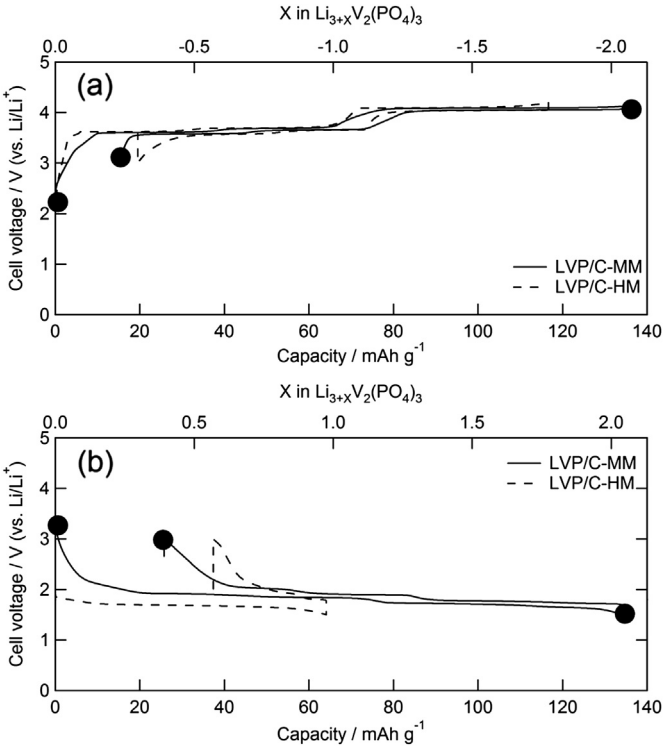

Fig. 2. The charge–discharge curves of (a) the cathode (V^{3+}/V^{4+} redox couple) and (b) the anode (V^{2+}/V^{3+} redox couple) for the carbon-coated LVP using a mechanical milling method (LVP/C-MM, solid line) and a hand milling method (LVP/C-HM, broken line) against Li anode with 1 M $LiPF_6$/EC + DMC (1:1). The symbols (●) represent the sampling points for the *ex situ* XRD measurement (Figs. 3 and 4).

We investigated the structure change of LVP/C-MM for the first charge and discharge cycle with V^{3+}/V^{4+} and V^{2+}/V^{3+} redox couple by *ex-situ* XRD measurements. The XRD measurements were performed on three samples of LVP/C-MM pellets during the charge and discharge cycle, as shown in Fig. 2.

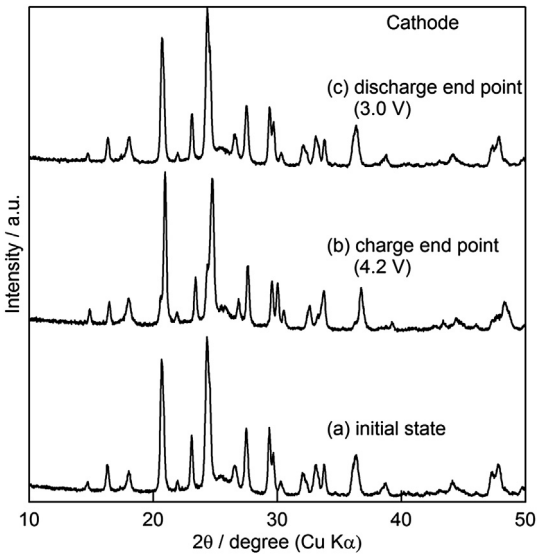

Fig. 3. The XRD patterns of LVP/C-MM cathode pellets during the first charge/discharge cycle; (a) the initial state, (b) the charge end point (4.2 V) and (c) the discharge end point (3.0 V).

Table 2
The lattice constants of LVP during the first charge–discharge process.

		a (Å)	b (Å)	c (Å)	β (°)	V (Å^3)
Cathode	Initial state	8.62	8.60	12.06	90.6	899.0
	Charge end point (4.2 V)	8.62	8.46	11.90	90.2	867.8
	Discharge end point (3.0 V)	8.62	8.60	12.05	90.6	893.2
Anode	Initial state	8.62	8.60	12.05	90.6	893.2
	Discharge end point (1.5 V)	8.54	8.65	12.07	90.7	891.6
	Charge end point (3.0 V)	8.63	8.61	12.07	90.6	896.8

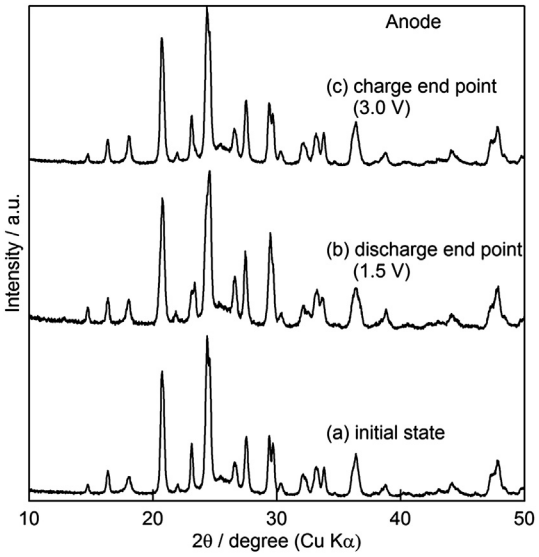

Fig. 4. The XRD patterns of LVP/C-MM anode pellets during the first discharge/charge cycle; (a) the initial state, (b) the discharge end point (1.5 V) and (c) the charge end point (3.0 V).

3.3. Structure change of LVP during the charge and discharge cycle against Li anode with non-aqueous electrolyte

Fig. 3 compares the XRD profiles of LVP/C-MM cathode pellets at (a) the initial state, (b) the charge end point (4.2 V) and (c) the discharge end point (3.0 V). All XRD diffraction peaks shifted to a higher 2θ angle from that of the initial state in the initial charge process, and moved back to almost the original position after the first discharge process. In particular, the XRD diffraction peaks of (0 2 0) and (0 0 4) moved markedly to a higher 2θ angle from that of the initial state in the first charge process. The lattice constants of LVP during the first charge–discharge process were calculated using PDXL program (Rigaku), as shown in Table 2. These results suggest that the *a*-axis in LVP structure was unchanged, while the *b*- and *c*-axes contracted. The unit cell volume change during the initial charge cycle was −2.9%.

Fig. 4 compares the XRD profiles of LVP/C-MM anode pellets at (a) the initial state, (b) the charge end point (1.5 V) and (c) the discharge end point (3.0 V). The XRD diffraction peaks of (0 2 0), (0 2 1) and (0 0 4) moved to a lower 2θ angle from that of the initial state in the initial discharge process. This result means that the *b*- and *c*-axes in the LVP structure were extended by the insertion of lithium. In contrast, the *a*-axis was hardly seen to extend and contract with the insertion of lithium, as shown in Table 2. Two Li ions insert into $Li_3V_2(PO_4)_3$ with the reduction from V^{3+} to V^{2+}. On the other hand, according to Voronoi diagram, a $Li_3V_2(PO_4)_3$ molecule has six empty 4e sites larger than lithium ion radius (0.76 Å). Among the six empty 4e sites in Fig. 5, the most possible Li insertion sites during the V^{3+}/V^{2+} redox reaction are site 5 and site 6 with the largest cavity. Because, the unit cell volume of the electrode was hardly changed even after 2Li insertion as shown in Table 2.

3.4. Electrochemical properties for LVP symmetric cell with non-aqueous electrolyte and all solid-state Li-ion batteries

Fig. 6 shows the charge–discharge curves for the LVP symmetric cell (cathode/anode weight balance 1:1) with 1 M $LiPF_6$/EC + DMC

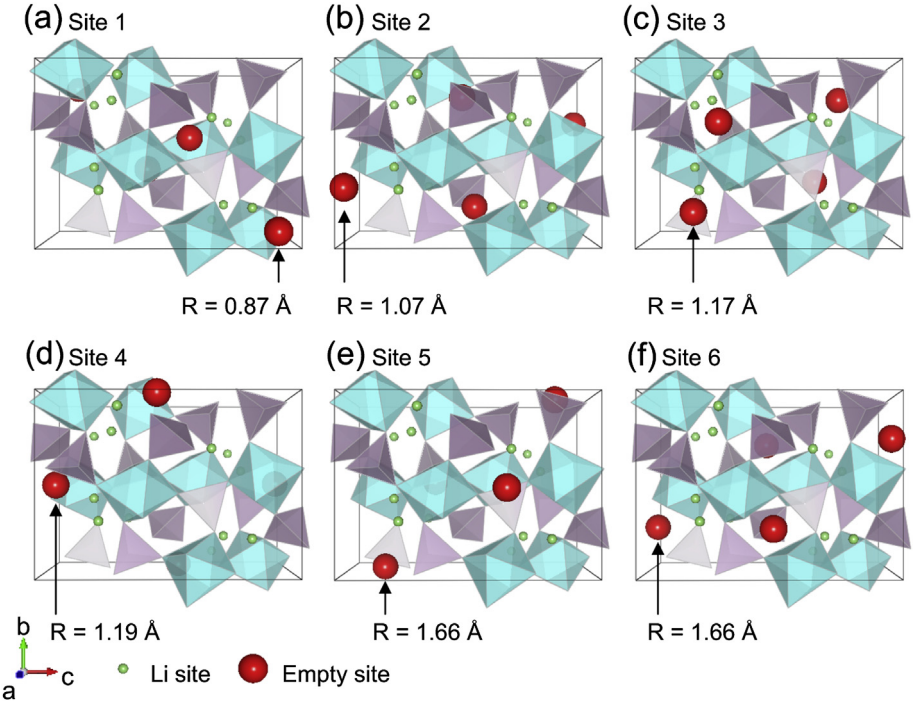

Fig. 5. The calculated empty sites (a)–(f) in LVP unit cell using a Voronoi diagram. The Li site and the empty site are shown a symbol, receptivity. "R" shows the radius of empty site.

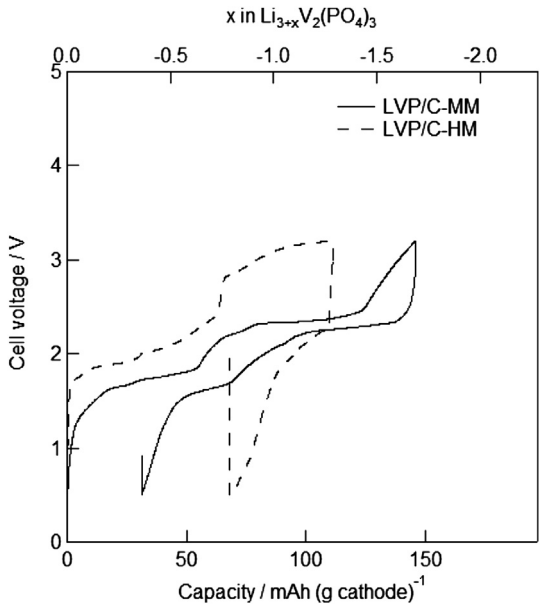

Fig. 6. The charge–discharge curves for the LVP symmetric cell of LVP/C-MM (solid line) and LVP/C-HM (broken line) with 1 M $LiPF_6$/EC + DMC (1:1 in volume) in the potential window between 0.5 and 3.0 V at the rate of 7.5 mA g^{-1} (0.2 mA cm^{-2}).

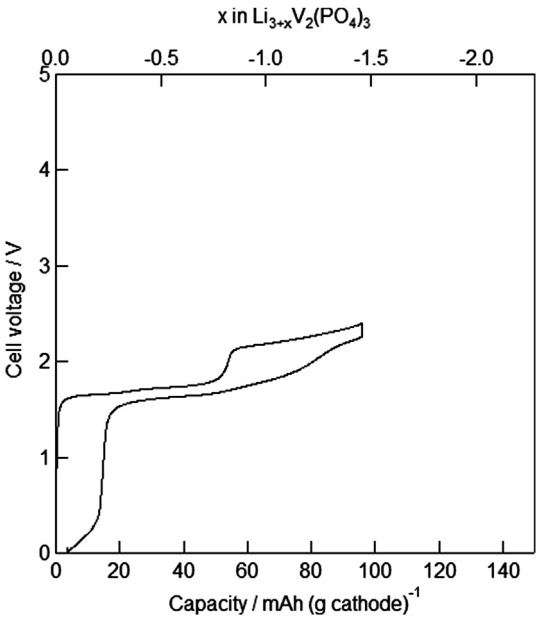

Fig. 8. The initial charge and discharge curves for the LVP/LAGP/LVP symmetric all solid-state battery of cathode/anode weight balance 1:1 at the rate of 6.1 mA g^{-1} (8.8 μA cm^{-2}) with the potential window between 0.0 and 2.4 V.

(1:1 in volume) in the potential window between 0.5 and 3.0 V at a rate of 7.5 mA g^{-1} (0.2 mA cm^{-2}). The initial charge and discharge capacity per cathode weight for LVP/C-HM were 111 mAh g^{-1} and 43 mAh g^{-1}, respectively, with a 39% discharge/charge efficiency. In contrast, these for LVP/C-MM were 145 mAh g^{-1} and 114 mAh g^{-1}, respectively, with a 79% discharge/charge efficiency. These findings demonstrated that the irreversible capacity of the LVP symmetric cell was improved as well as LVP versus Li metal by mechanical milling process.

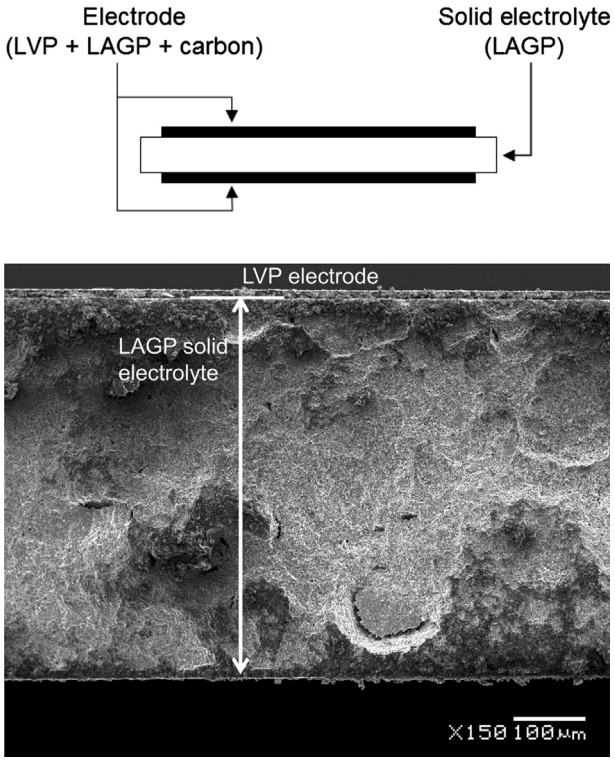

Fig. 7. The diagrammatic illustration and SEM images of the LVP/LAGP/LVP all solid-state cells.

Based on these results, we constructed an LVP/LAGP/LVP symmetric all solid-state battery, as shown in Fig. 7. The initial charge and discharge curves of the LVP/LAGP/LVP symmetric all solid-state battery with the cathode/anode weight balance 1:1 is shown in Fig. 8. The electrochemical measurements were carried out with the potential window between 0.0 and 2.4 V at a rate of 6.1 mA g^{-1} (8.8 μA cm^{-2}). The initial discharge capacity per cathode was 92 mAh g^{-1}. In a previous study [8], we fabricated an LVP/LAGP/LVP symmetric all solid-state battery using hand milling; the discharge capacity per cathode weight was only 40 mAh g^{-1} at a rate of 6.4 mA g^{-1} (8.8 μA cm^{-2}). The improvement of the electrochemical properties of the LVP/LAGP/LVP all solid-state Li-ion battery has succeeded by increased electroconductivity.

4. Conclusions

We could improve the anode properties (V^{2+}/V^{3+} redox couple) of LVP by carbon coating using mechanical milling. The irreversible capacity of LVP during the first discharge and charge cycle was greatly decreased compared to that of carbon-coated LVP using hand milling. Based on these results, we constructed an LVP/LAGP/LVP symmetric all solid-state battery, which shows 96 mAh g^{-1} (charge capacity based on cathode weight) and 92 mAh g^{-1} (discharge capacity based on cathode weight), respectively. In addition, XRD measurements proved that LVP could proceed to Li extraction/insertion by the reversible expansion/contraction of lattice due to the structure strength and flexibility of the corner-sharing NASICON matrix.

References

[1] U.V. Sacken, E. Nodwell, A. Sundher, J.R. Dahn, J. Power Sources 54 (1995) 240.
[2] P.G. Balakrishnan, R. Ramesh, T.P. Kumar, J. Power Sources 155 (2006) 401.
[3] J. Xie, N. Imanishi, T. Zhang, A. Hirano, Y. Takeda, O. Yamamoto, J. Power Sources 192 (2008) 689.
[4] H. Kitaura, A. Hayashi, K. Tadanaga, M. Tatsumisago, J. Electrochem. Soc. 156 (2009) A114.

[5] N. Kamaya, K. Homma, Y. Yamakawa, M. Hirayama, R. Kanno, M. Yonemura, T. Kamiyama, Y. Kato, S. Hama, K. Kawamoto, A. Mitsui, Nat. Mater. 10 (2011) 682.
[6] Y. Inda, T. Katoh, M. Baba, J. Power Sources 174 (2007) 741.
[7] A. Sakuda, H. Kitaura, A. Hayashi, K. Tadanaga, M. Tatsumisago, J. Power Sources 156 (2008) A27.
[8] E. Kobayashi, L.S. Plashnitsa, T. Doi, S. Okada, J. Yamaki, Electrochem. Comm. 12 (2010) 894.
[9] H. Aono, E. Sugimoto, Y. Sadaoka, N. Imanaka, G. Adachi, Bull. Chem. Jpn. 65 (1992) 2200.
[10] S.-C. Yin, H. Grondey, P. Strobel, M. Anne, L.F. Nazar, J. Am. Chem. Soc. 125 (2003) 10403.
[11] S. Patoux, C. Wurm, M. Morcrette, G. Rousse, C. Masquelier, J. Power Sources 19 (2003) 278.
[12] F. Izumi, K. Momma, Solid State Phenom. 130 (2007) 15.
[13] S.-C. Yin, P.S. Strobel, H. Grondey, L.F. Nazar, Chem. Mater. 16 (2004) 1465.